Available online at www.sciencedirect.com

ScienceDirect

Procedia Structural Integrity 41 (2022) 260–265

Structural Integrity Procedia

www.elsevier.com/locate/procedia

2nd Mediterranean Conference on Fracture and Structural Integrity

# Crack path estimation in the shot-earth 772 by a discrete element method

Angélica Colpo[a], Sabrina Vantadori[b]*, Leandro Friedrich[c], Andrea Zanichelli[b], Camilla Ronchei[d], Daniela Scorza[e], Ignacio Iturrioz[a]

[a]*Program of Mechanical Pos-Graduation, Federal University of Rio Grande do Sul, Sarmento Leite 425, 90040-060 Porto Alegre, Brazil*
[b]*Department of Engineering & Architecture, University of Parma, Parco Area delle Scienze 181/A, 43124 Parma, Italy*
[c]*Department of Mechanical Engineering, Federal University of Pampa, Av. Tiaraju 810, 97546-550 Alegrete, Brazil*
[d]*Department of Civil Engineering, University of Calabria, via Pietro Bucci, 87036 Arcavacata di Rende (CS), Italy*
[e]*Department of Engineering, University of Naples Parthenope, Centro Direzionale Isola C4, 80143 Napoli, Italy*

**Abstract**

In the present paper, the fracture behaviour of the shot-earth 772, in terms of crack path, is numerically investigated. To such an aim, a version of the lattice discrete element method is used to numerically simulate fracture toughness testing performed, on the shot-earth 772, by employing the Modified Two-Parameter model.
A comparison between the numerical crack path and the experimental ones is performed, highlighting as the lattice discrete element method is able to capture the kinked crack shape, typical of quasi-brittle materials.



*Keywords:* Quasi-brittle materials; Crack path estimation; Discrete Element Method; Modified Two Parameter Model.

## 1. Introduction

Europe has an extensive history of earth constructions and a wide variety of technologies, where many of such technologies have been exported to other areas of world (Hall et al. (2012)).

In such a context, the shot-earth is a novel technology where the material, composed by stabilised or unstabilised soil, aggregates and water, is pneumatically projected at high velocity onto a receiving surface (Curto et al. (2020)).

* Corresponding author.
*E-mail address:* sabrina.vantadori@unipr.it


10.1016/j.prostr.2022.05.030

The material investigated in the present paper is a specific mixture of the shot-earth, where the soil is stabilised by cement, and named shot-earth 772, being characterised by a proportion of soil: sand: cement equal to 7:7:2.

The aim of the present paper is to numerically simulate the crack path experimentally observed during fracture toughness testing, performed according to the Modified Two-Parameter Model (Vantadori et al. (2016)). The simulation is carried-out by employing a version of the lattice discrete element method, originally proposed by Riera (1984).

The paper is structured as follows: in Section 2 the main concepts of the lattice discrete element method (LDEM) are presented. Section 3 describes the experimental fracture tests performed on the short-earth 772, whereas the LDE model here employed is presented in Section 4. Section 5 is dedicated to present the results obtained in terms of crack path, whereas the main conclusions are summarized in Section 6.

## 2. Lattice discrete element method (LDEM)

The LDEM allows us to model a continuous medium as a 3D-array of nodes, linked by massless uniaxial elements (also named bars), which are only able to transfer axial load. The discretised masses are assumed concentrated at the above nodes. More precisely, the discretization strategy employs a basic cubic module, built with twenty bars and nine nodes (Fig. 1a). The lengths of the longitudinal and diagonal elements are $L_n = L_{co}$ and $L_d = \left(\sqrt{3}/2\right) L_{co}$, respectively (Kosteski (2012)). Each node has three degrees of freedom.

The system of equations resulting from applying the Newton's second law to each node, is given by:

$$\boldsymbol{M}_{ij}\ddot{\boldsymbol{x}}_j + \boldsymbol{C}_{ij}\dot{\boldsymbol{x}}_j + \boldsymbol{F}_i(t) - \boldsymbol{P}_i(t) = 0 \tag{1}$$

where the vectors $\ddot{\boldsymbol{x}}_j$ and $\dot{\boldsymbol{x}}_j$ represent the nodal acceleration and velocity, respectively, $\mathbf{M}_{ij}$ and $\mathbf{C}_{ij}$ are the mass and damping matrices, respectively, and the vectors $\mathbf{F}_i(t)$ and $\mathbf{P}_i(t)$ are the internal and external nodal forces, respectively. Since $\mathbf{M}_{ij}$ and $\mathbf{C}_{ij}$ are diagonal matrices, the Eq. (1) are not coupled, and can be integrated in the time domain using an explicit finite difference scheme.

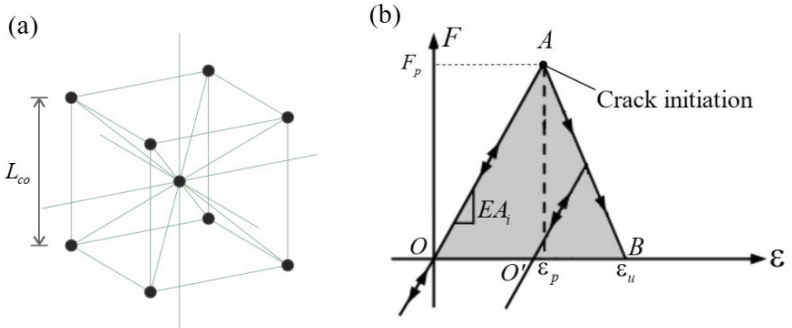


Fig. 1. (a) Basic cubic module employed in the discretization; (b) bilinear constitutive law of each bar.

The possibility of bars breaking is considered through the bilinear law show in Fig. 1b.

The total mass of the basic cubic module is equal to $m = \rho L_n^3$, being $\rho$ the mass density of the material and $L_n^3$ the volume of the module. In the bilinear law shown in Fig. 1b, $EA_i$ is the bar specific stiffness, where $E$ is the Young modulus, $A_i$ is the cross-section area of the bar, $\varepsilon_p$ is the critical strain (when the bar starts to damage) and $\varepsilon_u$ is the strain value for which the element loses its load bearing capacity (that is, the bar breaks).

Successful applications of such a method are available in the literature (Iturrioz et al. (2013), Colpo et al. (2016), Birck et al. (2019), Zanichelli et al. (2021)).

## 3. Fracture toughness testing

According to the MTPM (Vantadori et al., (2016); Carpinteri et al. (2017)) and the RILEM Recommendations (RILEM (1990)), the specimens are tested under three-point bending loading and crack mouth opening displacement (CMOD) control (Fig. 2). The specimen presents a prismatic shape with a notch in the lower part of the middle cross-section (Fig. 2). The geometric sizes of the specimen are function of the width B, that is: depth $W = 2B$, span $S = 8B$ and notch depth $a_0 = 2/3\,B$.

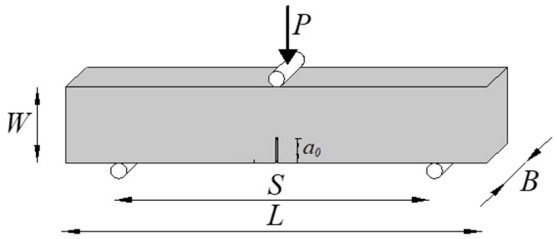


Fig. 2. Specimen geometry and loading configuration.

The specimen is monotonically loaded up to the peak load and, in the post-peak stage, when the force is equal to 95% of peak load, the specimen is fully unloaded. After that, the specimen is reloaded up to failure.

Five specimens are tested. The mean values of the corresponding geometrical sizes are listed in Table 1, together with the value of Young Modulus, *E*, and fracture toughness, $K^{S}_{(I+II)C}$. Note that these latter parameters are computed according to the MTPM (interested readers may refer to Zanichelli et al. (2018) and Vantadori et al. (2021)).

Table 1. Mean values of specimen sizes, elastic modulus and fracture toughness.

| | $W$ (mm) | $B$ (mm) | $a_0$ (mm) | $L$ (mm) | $S$ (mm) | $E$ (MPa) | $K^{S}_{(I+II)C}$ (MPa.m$^{0.5}$) |
|---|---|---|---|---|---|---|---|
| Mean value | 77.01 | 44.51 | 27.15 | 375.00 | 320.00 | 6918.11 | 0.29 |

Moreover, the failure configurations observed during the experimental campaign are reported in Figure 3.

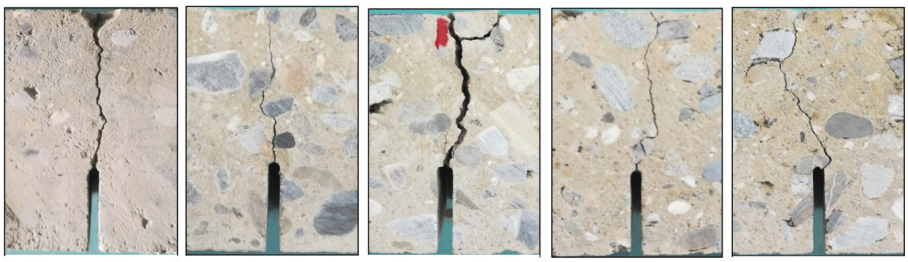


Fig. 3. Experimental failure configurations.

## 4. Numerical model

Using the LDEM, a 3D model is built and calibrated by employing both the sizes and the properties listed in Table 1. In Table 2 the parameter of the discretization adopted are reported, where $N_{i\ (i=x,y,z)}$ is the modules number along x, y and z direction, respectively, $L_{co}$ is the cubic module size, $\rho$ is the mass density, $\nu$ is the Poisson coefficient and $G_f$ is the fracture energy.

Table 2. Parameters characterising the 3D numerical model.

| $L_{co}$ [mm] | $N_x$ [-] | $N_y$ [-] | $N_z$ [-] | $\rho$ [kg/m$^3$] | $\nu$ [-] | $G_f$ [N/m] |
|---|---|---|---|---|---|---|
| 2.00 | 188 | 38 | 22 | 2070 | 0.25 | 18.65 |

Note that, in correspondence of the left support of the model the nodes are constrained in both *x* and *y* directions, whereas in correspondence of the right support they are constrained in *y* direction (Fig. 4a). In correspondence of the upper region of the model show in Fig. 4b, characterised by $x = L/2$, a prescribed displacement, $U_y(t)$, in the -*y* direction is applied.

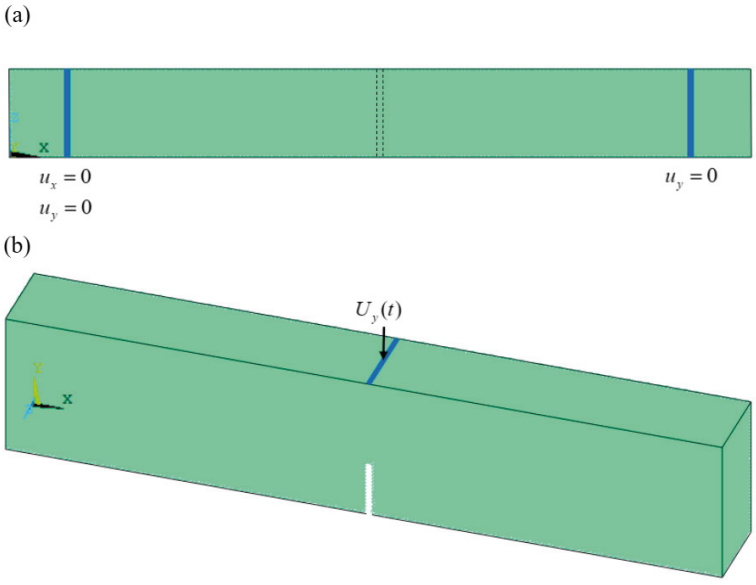


Fig. 4. (a) Bottom view of the model; (b) model geometry and applied loading.

## 5. Results

Fig. 5 shows the failure configuration of the model, where the green bars are the undamaged bars, the orange ones are the damaged bars and the red ones are the broken bars. As previously described, the LDEM allows to capture the crack path due to its ability to deactivate bars at a strain value equal to $\varepsilon_u$ (see Fig.1(b)).

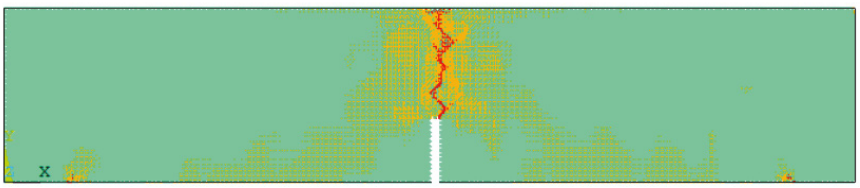

Fig. 5. Numerical failure configuration.

By comparing the numerical failure configuration with the failure configurations obtained during the experimental campaign (Fig. 3), it can be observed that the agreement between crack paths is quite satisfactory, being the model able to capture the kinked cracks shape experimentally found. For a detailed comparison, the kinked crack profile related to the specimens No. 1 and No. 3 are shown in Fig. 6 together with the numerical one, thus highlighting a good correlation.

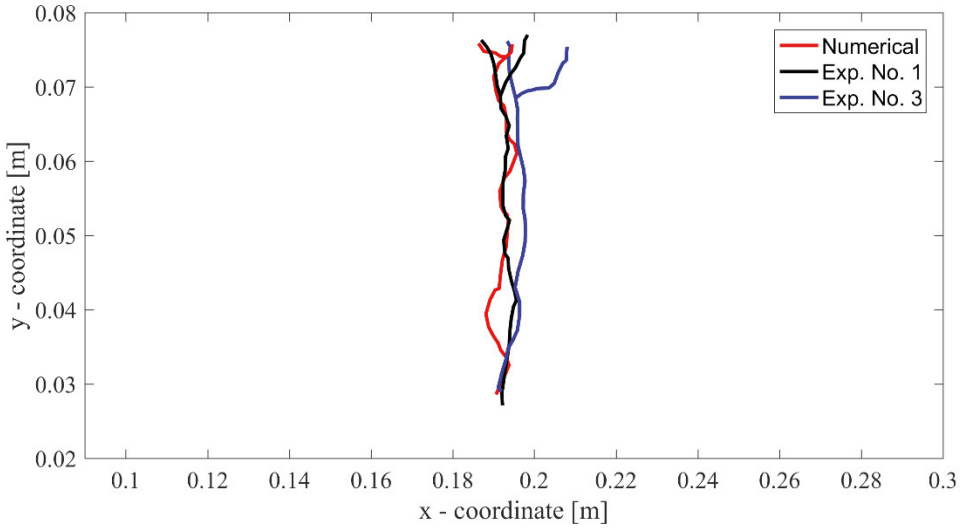


Fig. 6. Comparison between numerical and experimental crack paths.

Furthermore, by dividing the model in 2 parts along the thickness direction, it possible to observe how the crack path changes along the thickness of the specimen (Fig. 7).

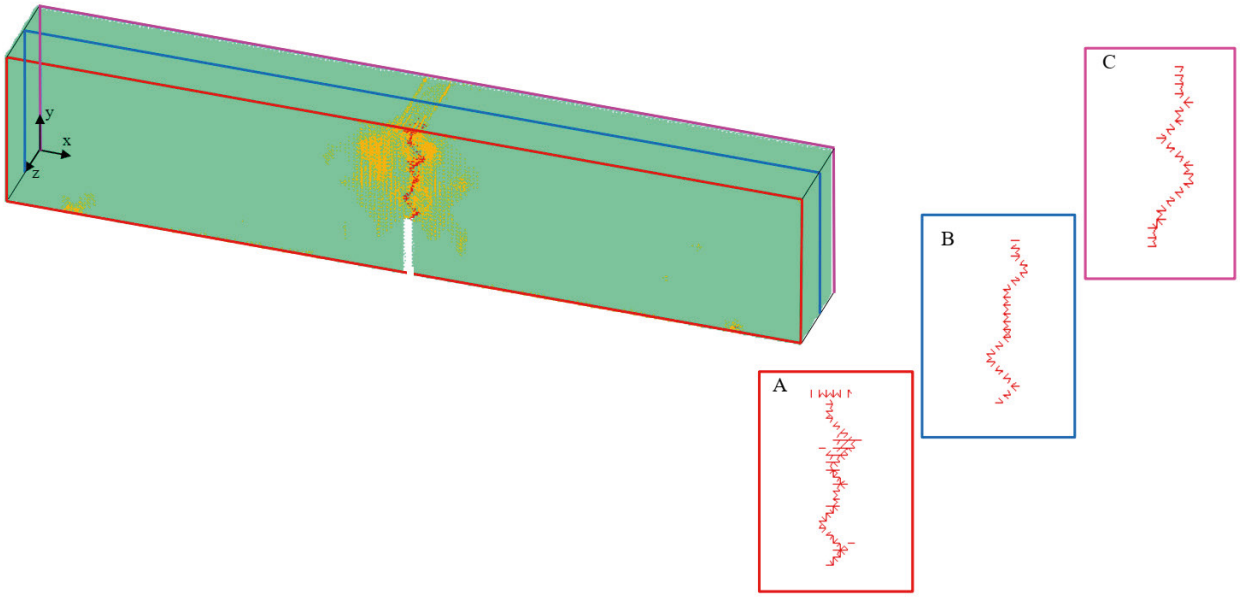


Fig. 7. Numerical crack paths along the thickness direction: A is in correspondence of $z = B$ , B is in correspondence of $z = B/2$ , C is in correspondence of $z = 0$ .

## 6. Conclusions

In the present paper, the fracture behaviour of the shot-earth 772 has been numerically investigated. More precisely, a version of the LDEM has been employed to simulate the experimental crack paths observed during fracture testing. Note that such tests have been performed on the short-earth 772, in accordance to the Modified Two-Parameter Model.

The obtained numerical crack path has been compared with the experimental ones. It has been observed that the developed model is able to capture the kinked crack shape (typical of quasi-brittle material) with a high accuracy, being the crack profiles, estimated and experimental, very similar among them.

## Acknowledgements

The authors wish to thank the Italian Ministry of University and Research (supporting the present research with the project FISR2019_00245, First National Grant 2019), the National Council for Scientific and Technological Development (CNPq—Brazil) and Coordination for the Improvement of Higher Education Personnel (CAPES—Brazil).

## References

Birck G., Rinaldi A., Iturrioz I., 2019. The fracture process in quasi-brittle materials simulated using a lattice dynamical model. Fatigue & Fracture of Engineering Materials & Structures, 42, 12, 2709-2724.

Carpinteri A, Fortese G, Ronchei C, Scorza D, Vantadori S., 2017. Mode I fracture toughness of fibre reinforced concrete. Theoretical and Applied Fracture Mechanics, 91, 66-75.

Colpo A.B., Kosteski L.E., Iturrioz I., 2016. The size effect in quasi-brittle materials: Experimental and numerical analysis. International Journal of Damage Mechanics, 26, 395-416.

Curto A., Lanzoni L., Tarantino A.M., Viviani M., 2020. Shot-earth for sustainable constructions. Construction and Building Materials, 239. 2020.

Hall M.R., Lindsay R., Krayenhoff M., 2012. Modern earth buildings: Materials, engineering, constructions and applications. Woodhead Publishing.

Iturrioz I., Lacidogna G., Carpinteri A., 2013. Experimental analysis and truss-like discrete element model simulation of concrete specimens under uniaxial compression. Engineering Fracture Mechanics, 110, 81-98.

Kosteski L., 2012. Application of the lattice discrete elements method in the study of structural collapse. Doctoral Thesis, Federal University of Rio Grande do Sul.

Kosteski L.E., Iturrioz, I., Barrios, D.R, 2012. Crack propagation in elastic solids using the truss-like discrete element method. Int. J. Fracture (Print) 174, 139-161.

Riera J.D, 1984. Local effects in impact problems on concrete structures. Proceedings, Conference on structural analysis and design of nuclear power plants, Porto Alegre, Brazil 3, 57-79.

RILEM Technical Committee, 89-FMT, 1990. Determination of fracture parameters (KsIC and CTODc) of plain concrete using three-point bend tests, proposed RILEM draft recommendations. Materials and Structures, 23, 457–460.

Vantadori, S., Carpinteri, A., Fortese, G., Ronchei, C., Scorza, D, 2016. Mode I fracture Toughness of fibre-reinforced concrete by means of a modified version of the two-parameter model. Procedia Structural Integrity 2, 2889-2895.

Vantadori S., Carpinteri A., Głowacka K., Greco F., Osiecki T., Ronchei C., Zanichelli A., 2021. Fracture toughness characterisation of a glass fibre-reinforced plastic composite. Fatigue and Fracture of Engineering Materials and Structures, 44, 1, 3-13.

Zanichelli A., Carpinteri A., Fortese G., Ronchei C., Scorza D., Vantadori S., 2018. Contribution of date-palm fibres reinforcement to mortar fracture toughness. Procedia Structural Integrity, 13, 542-547.

Zanichelli A., Colpo A., Friedrich L., Iturrioz I., Carpinteri A., Vantadori S., 2021. A Novel Implementation of the LDEM in the Ansys LS-DYNA Finite Element Code. Materials, 14, 7792.